In vivo evaluation of cerebral venous sinus morphology using pulsed-laser-diode-based desktop photoacoustic tomography system

Rajendran, Praveenbalaji; Sahu, Samiran; Dienzo, Rhonnie Austria; Pramanik, Manojit

2020

Rajendran, P., Sahu, S., Dienzo, R. A., & Pramanik, M. (2020). In vivo evaluation of cerebral venous sinus morphology using pulsed-laser-diode-based desktop photoacoustic tomography system. Proceedings of SPIE - Photons Plus Ultrasound: Imaging and Sensing 2020, 11240, 107-. doi:10.1117/12.2543892

https://hdl.handle.net/10356/146565

https://doi.org/10.1117/12.2543892

In vivo evaluation of cerebral venous sinus morphology using pulsed-laser-diode-based desktop photoacoustic tomography system

Praveenbalaji Rajendran[1], Samiran Sahu[2], Rhonnie Austria Dienzo[1] and Manojit Pramanik*[1]
[1]School of Chemical and Biomedical Engineering, Nanyang Technological University, Singapore;
[2]Visited Nanyang Technological University, Singapore as an intern student through NTU-India Connect Research Internship Program from Indian Institute of Technology, Kharagpur, India

ABSTRACT

Assessment of morphological changes in cerebral venous sinus of small animal models is important to gain insights of various disease conditions such as intracranial hypotension, Idiopathic intracranial hypertension (IIH), Cerebral venous sinus thrombosis, subdural hematoma etc. Photoacoustic Tomography (PAT), a fast-growing non-invasive hybrid imaging modality which combines high optical contrast and resolution in deep tissue imaging offers a novel, rapid and cost-effective way to analyze the morphological changes of venous sinus in comparison with the conventional imaging modalities. In this study, we examined the morphological changes of sagittal sinus in the rat brain due to intracranial pressure changes induced by Cerebrospinal fluid (CSF) extraction using low cost pulsed laser diode (PLD) based desktop (PAT) system. Our results indicate that the desktop PLD-PAT system can be employed to evaluate the changes in the cerebral venous sinus in preclinical models. We observed a ~30% average increase in the area of sagittal venous sinus from the baseline, when the CSF is extracted.

Keywords: photoacoustic imaging, cerebral venous sinus, cerebrospinal fluid, pulsed laser diode.

1. INTRODUCTION

Cerebral venous sinus is an important component of the human brain embedded between the endosteal and meningeal layers of the dura are. It serves as the major drainage of cerebral blood flow and as the prime site of cerebrospinal fluid (CSF) reabsorption [1]. Understanding the morphology of cerebral venous sinus is important to gain insights in to various clinical pathologies such as cerebral venous thrombosis (CVT), hemorrhages, hydrocephalus, intracranial hypotension (IH) etc. [2-4]. In current scenario, the preferred imaging modality to analyze the morphological changes of cerebral venous sinus is magnetic resonance imaging (MRI) [5]. However, MRI is expensive and has limitations like low temporal resolution and longer imaging time. Photoacoustic tomography (PAT), a rapidly evolving hybrid imaging modality combining high ultrasonic resolution and optical contrast offers a cost-effective means to analyze the changes in cerebral venous sinus in small animal models [6-14]. In PAT, a nanosecond laser pulse irradiates the sample containing optical absorbers. The absorption of light by the optical absorbers causes a local temperature rise resulting in the generation of photoacoustic waves. These PA waves are then acquired around the sample by employing a wide band ultrasonic transducer (UST). The acquired signals are then reconstructed in to photoacoustic images by using various reconstruction algorithms [15-19].

Photo luminescence diodes (PLD) as excitation sources for PAT is gaining a lot of attention in recent years due to its high repetition rate, low cost and compact size in comparison with the conventional bulky Nd:YAG based laser excitation sources [20-25]. PAT imaging systems using PLD as excitation sources was already demonstrated for numerous applications such as brain imaging, high frame rate imaging, cardiovascular diseases and rheumatological disorders [23, 26, 27]. Employing the UST's in vertical configuration by coupling acoustic reflectors instead of using UST's in horizontal configuration reduces the scanning radius of the PAT, thereby rendering the PAT imaging system furthermore compact [28]. A comparative study on the performance of SUTR and UST was demonstrated using OPO-PAT system [29]. In this study a PLD based PAT system was used to examine the morphological changes in the sagittal sinus of the rat brain induced through CSF extraction.

* Email: manojit@ntu.edu.sg

2. PLD-PAT SYSTEM

The schematic of the PLD-PAT system used in this study is shown in the Fig. 1(a). A ~816 nm wavelength PLD capable of delivering ~107 nm width pulses at 2KhZ repetition rate was mounted at the center of the circular scanning system. The PLD was controlled by the laser driving unit comprising of a function generator, a 12 V low voltage power supply, a variable high voltage power supply and a water-cooling unit. The laser beam generated by the PLD was homogenized using diffuser before irradiating the head of the animal. The area of the laser spot size irradiating the animal head was ~20 cm2. The fluence of the irradiating beam was maintained in par with the American National Standards Institute (ANSI) safety limit (~0.17 mJ/cm2) for a scan time of 12 seconds [30]. The animal was mounted on a custom-made holder as shown in the Fig 1(a). A 5 MHz center frequency (13 mm active area, 70% fractional bandwidth) unfocused UST coupled with acoustic reflector (SUTR) was used to acquire the generated PA waves. The SUTR was immersed in the water for better ultrasound coupling between the PA waves and the SUTR. The SUTR was driven by the stepper motor 360˚ around the head of the animal to acquire the generated PA waves. The PA signals were then amplified by a low noise signal amplifier of 48 dB and then digitized, stored inside the computer (Intel Xeon, 3.7 GHz 64-bit processor, 16 GB RAM) by a data acquisition (DAQ) card (Spectrum, M2i.4932-Exp).

.

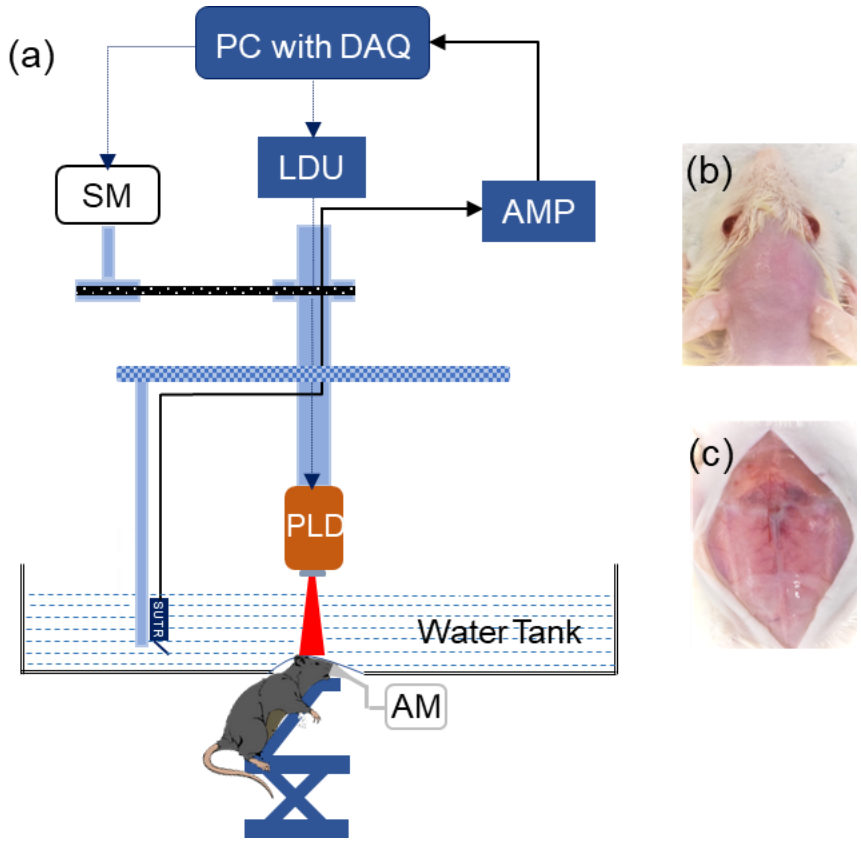

Fig. 1. (a) PLD-PAT imaging setup for noninvasive brain imaging: SUTR-single-element ultrasound transducer with reflector; AMP-amplifier; SM-stepper motor; PLD-pulsed laser diode; LDU-laser driving unit; AM-anesthesia machine; PC-personal computer; DAQ-data acquisition card. Image of the rat head (b) hair removed before PA imaging (d) open scalp after the animal was euthanized.

3. PREPARATION OF ANIMAL FOR BRAIN IMAGING

Two NTac: Sprague Dawley®SD® female rats (weighing ~90 ± 5 gms) procured from InVivos Pte. Ltd, Singapore were utilized for the in vivo study. The rats were divided into two groups: control group and CSF group. The rats were anesthetized by a combination of Ketamine (100 mg/ml) and Xylazine (20 mg/ml) before the imaging. The hair on the rat head was removed by using depilatory cream, eye gel was applied on both the eyes and ultrasound gel was applied for better coupling of the acoustic waves. The rat was placed in an upright position on a customized holder and its body was secured using surgical tape. The anesthesia was maintained over the entire course of the experiment by a continuous inhalation of 0.75% isoflurane and 1.0 L/min oxygen. The rat head was positioned on the imaging plane using a translational stage. On the termination of experiments the rat was euthanized by intraperitoneal administration of Valabarb (sodium pentobarbitone 300 mg/ml). The rat head with scalp open is shown in Figure 1(c).

4. INDUCTION OF MORPHOLOGICAL CHANGES

The morphological change in the cerebral venous sinus of the rat was induced by establishing a medical phenomenon called as intracranial hypotension (IH) [31, 32]. The IH was incited by removing the CSF from the cisterna magna of the rat in the CSF group. A volume of ~45±5 µl CSF was removed by a needle connected to the draw syringe. CSF extraction without the contamination of blood was ensured during the extraction.

5. IN VIVO BRAIN IMAGING

In vivo brain imaging was performed on the rats prepared as discussed in section 2 using the PLD-PAT system by circularly scanning the SUTR for 12 seconds around the sample. For the rat in the CSF group, 8 brain images before the CSF extraction and 28 brain images after the CSF extraction was obtained at an interval of 4 minutes and for the rat in the control group 16 brain images were obtained at an interval of 10 minutes. The duration of the experiments in both the case were ~180 minutes. The cross-sectional brain images obtained using PLD-PAT system is shown in Fig. 2.

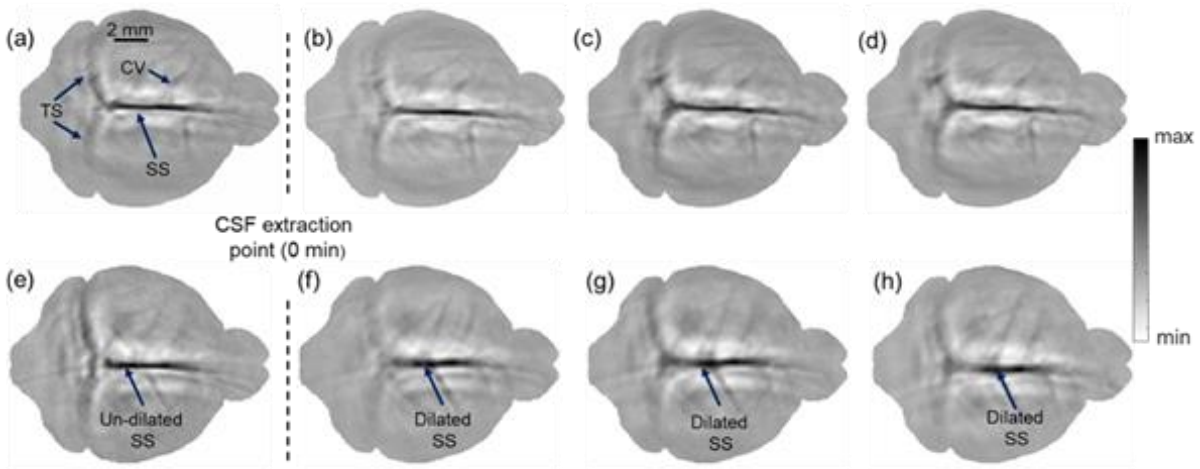

Fig. 2. (a) In vivo PLD-PAT images of the rat brain: images of the rat in the control group at (a) -30 minutes, (b) 10 minutes, (c) 60 minutes and (d) 120 minutes. Brain images of the rat in the CSF group (e) before CSF extraction (-28 minutes), (f) 5 minutes, (g) 59 minutes and (h) 117 minutes post CSF extraction. Herein, SS, sagittal sinus; TS, transverse sinus; CV, cerebral veins.

6. RESULT AND DISCUSSION

The PA brain images of the control group pre and post CSF extraction is shown in Figs. 2(a-d). The PA brain images of the CSF group pre and post CSF extraction is shown in Figs. 2(e-h). A morphological change that occurs in the cerebral venous sinus to maintain the hemostasis following the CSF extraction is venous sinus distension. The cerebral venous distension provides a reliable clue to interpret various IH related pathologies such as hemorrhages, hydrocephalus etc. The morphological changes in the contour of the cerebral venous sinus can be clearly noticed from the CSF group images obtained before and after CSF extraction. To interpret the results better, the area of the sagittal sinus region of the cerebral venous was calculated for both the CSF and control group rat. The SS area was calculated from the PA brain images by contrast enhancing using histogram equalization method followed by binarization with 50% of the maximum value as threshold. The region of interest (SS) was separated from the background and the number of pixels with binary value 1 was calculated and multiplied with the individual pixel area (0.625 mm2) to obtain the actual SS area. All the image processing was performed using MATLAB. The SS areas calculated for each rat in both the CSF and control group was normalized by dividing the SS areas at each time points with the initial SS area.

Fig. 3 shows graph of the normalized SS areas of the rat from the CSF group (blue circles) and the rat from the control group (black squares). From the plot it can be noticed that SS area after the CSF extraction in the CSF group is greater than the SS area before the CSF extraction, which is in correlation with visually noticeable changes between the pre and post CSF extraction images of the CSF group. Whereas for the rat in the control group the SS area remained almost similar throughout the entire duration of the experiment, the slight increasing trend in the SS area was due to the exposure of isoflurane over the long duration and persistent pressure over the head of the animal. The percentage difference in the SS area over the pre and post CSF extraction period was calculated, and it was found that the SS area increased by after the CSF extraction.

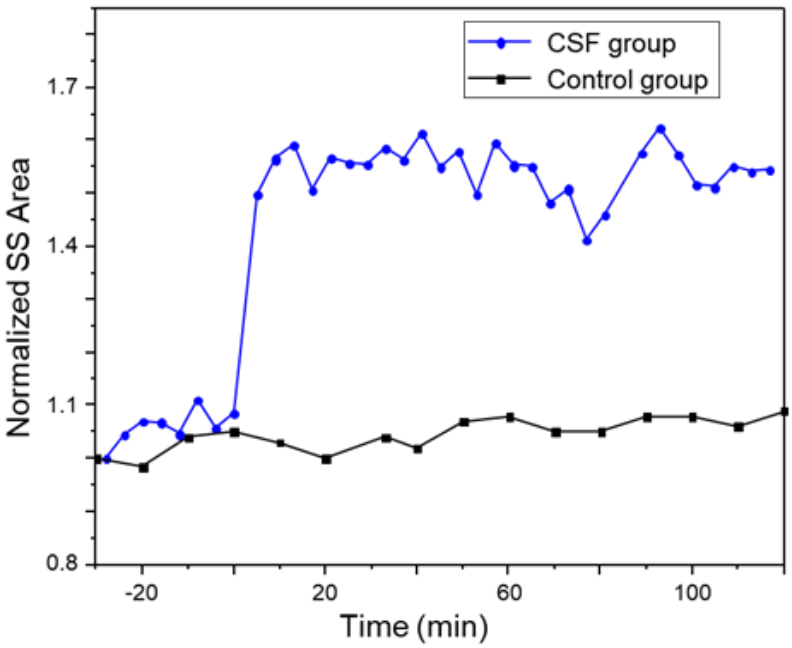

Fig. 3. Graph showing the Normalized sagittal sinus (SS) areas of the rat from the control group and the CSF group over the entire duration of the experiment.

7. CONCLUSION

In this study, the PLD-PAT systems capability to noninvasively assess the morphological changes of the cerebral venous sinus was demonstrated using a preclinical IH rat model. The IH was induced by the extraction of CSF from the cisterna magna of the rats. In vivo brain imaging using the PAT system was performed before and after IH induction to monitor the morphological changes in the cerebral venous sinus of the rat brain due to IH. The results and analysis demonstrate

that the PLD-PAT imaging system is capable of non-invasively detecting the contour change of the cerebral venous with high specificity. Before and after the IH occurrence. A change in the SS area by ~30% was observed after the induction of IH.

REFERENCES

[1] A. G. Caso V, Paciaroni M, *Handbook on Cerebral Venous Thrombosis*: Front Neurol Neurosci. Basel, Karger.

[2] E. Ferrante, V. Prone, F. Rubino, and M. Ferrante, "Spontaneous intracranial hypotension with chronic brain sagging causing foramen magnum CSF circulation disorder reversible after lumbar epidural blood patch," *Neurological Sciences*, vol. 39, pp. 1137-1138, 2018.

[3] S. Ade and M. Moonis, "Intracranial Hypotension with Multiple Complications: An Unusual Case Report," *Case Reports in Neurological Medicine*, vol. 2013, p. 3, 2013.

[4] S. Berroir, D. Grabli, F. Héran, P. Bakouche, and M. G. Bousser, "Cerebral Sinus Venous Thrombosis in Two Patients with Spontaneous Intracranial Hypotension," *Cerebrovascular Diseases*, vol. 17, pp. 9-12, 2004.

[5] J. L. Leach, R. B. Fortuna, B. V. Jones, and M. F. Gaskill-Shipley, "Imaging of Cerebral Venous Thrombosis: Current Techniques, Spectrum of Findings, and Diagnostic Pitfalls," *RadioGraphics*, vol. 26, pp. S19-S41, 2006.

[6] P. Wray, L. Lin, P. Hu, and L. V. Wang, "Photoacoustic computed tomography of human extremities," *Journal of Biomedical Optics*, vol. 24, pp. 1-8, 2019.

[7] W. Roll, N. A. Markwardt, M. Masthoff, A. Helfen, J. Claussen, M. Eisenblätter, *et al.*, "Multispectral optoacoustic tomography of benign and malignant thyroid disorders - a pilot study," *Journal of Nuclear Medicine*, pp. jnumed-118, 2019.

[8] M. Nishiyama, T. Namita, K. Kondo, M. Yamakawa, and T. Shiina, "Ring-array photoacoustic tomography for imaging human finger vasculature," *Journal of Biomedical Optics*, vol. 24, pp. 1-12, 2019.

[9] L. Li, L. Zhu, C. Ma, L. Lin, J. Yao, L. Wang, *et al.*, "Single-impulse Panoramic Photoacoustic Computed Tomography of Small-animal Whole-body Dynamics at High Spatiotemporal Resolution," *Nature Biomedical Engineering*, vol. 1, p. 0071, 2017.

[10] Y. Zhou, J. Yao, and L. V. Wang, "Tutorial on photoacoustic tomography," *Journal of Biomedical Optics*, vol. 21, p. 061007, 2016.

[11] J. Xia and L. V. Wang, "Photoacoustic Tomography of the Brain," in *Optical Methods and Instrumentation in Brain Imaging and Therapy*, S. J. Madsen, Ed., ed New York: Springer Science+Business Media, 2013.

[12] J. Xia, M. R. Chatni, K. Maslov, Z. J. Guo, K. Wang, M. Anastasio, *et al.*, "Whole-body ring-shaped confocal photoacoustic computed tomography of small animals in vivo," *Journal of Biomedical Optics*, vol. 17, p. 050506, 2012.

[13] X. Yang, A. Maurudis, J. Gamelin, A. Aguirre, Q. Zhu, and L. V. Wang, "Photoacoustic tomography of small animal brain with a curved array transducer," *Journal of Biomedical Optics*, vol. 14, p. 054007, 2009.

[14] C. Li and L. V. Wang, "Photoacoustic tomography of the mouse cerebral cortex with a high-numerical-aperture-based virtual point detector," *Journal of Biomedical Optics*, vol. 14, p. 024047, 2009.

[15] S. Schoeder, I. Olefir, M. Kronbichler, V. Ntziachristos, and W. A. Wall, "Optoacoustic image reconstruction: the full inverse problem with variable bases," *Proceedings of the Royal Society A: Mathematical, Physical and Engineering Sciences*, vol. 474, p. 20180369, 2018.

[16] Y. Han, L. Ding, X. L. D. Ben, D. Razansky, J. Prakash, and V. Ntziachristos, "Three-dimensional optoacoustic reconstruction using fast sparse representation," *Optics Letters*, vol. 42, pp. 979-982, 2017.

[17] S. K. Kalva and M. Pramanik, "Experimental validation of tangential resolution improvement in photoacoustic tomography using a modified delay-and-sum reconstruction algorithm," *Journal of Biomedical Optics*, vol. 21, p. 086011, 2016.

[18] D. Wang, Y. Wang, Y. Zhou, J. F. Lovell, and J. Xia, "Coherent-weighted three-dimensional image reconstruction in linear-array-based photoacoustic tomography," *Biomedical Optics Express*, vol. 7, pp. 1957-65, 2016.

[19] H. Grün, R. Nuster, G. Paltauf, M. Haltmeier, and P. Burgholzer, "Photoacoustic tomography of heterogeneous media using a model-based time reversal method," in *Proc SPIE*, 2008, p. 685620.

[20] P. K. Upputuri and M. Pramanik, "Photoacoustic imaging in the second near-infrared window: a review," *Journal of Biomedical Optics*, vol. 24, p. 040901, 2019.

[21] P. K. Upputuri and M. Pramanik, "Fast photoacoustic imaging systems using pulsed laser diodes: a review," *Biomedical Engineering Letters*, vol. 8, pp. 167-181, 2018.

[22] A. Hariri, A. Fatima, N. Mohammadian, S. Mahmoodkalayeh, M. A. Ansari, N. Bely, *et al.*, "Development of low-cost photoacoustic imaging systems using very low-energy pulsed laser diodes," *Journal of Biomedical Optics,* vol. 22, p. 075001, 2017.
[23] K. Sivasubramanian and M. Pramanik, "High frame rate photoacoustic imaging at 7000 frames per second using clinical ultrasound system," *Biomedical Optics Express,* vol. 7, pp. 312-323, 2016.
[24] L. Zeng, G. Liu, D. Yang, and X. Ji, "3D-visual laser-diode-based photoacoustic imaging," *Optics Express,* vol. 20, pp. 1237-46, 2012.
[25] L. Zeng, G. Liu, D. Yang, and X. Ji, "Cost-efficient laser-diode-induced optical-resolution photoacoustic microscopy for two-dimensional/three-dimensional biomedical imaging," *Journal of Biomedical Optics,* vol. 19, p. 076017, 2014.
[26] S. K. Kalva, P. K. Upputuri, P. Rajendran, R. A. Dienzo, and M. Pramanik, "Pulsed laser diode-based desktop photoacoustic tomography for monitoring wash-in and wash-out of dye in rat cortical vasculature," *Journal of Visualized Experiments,* vol. 147, p. e59764, 2019.
[27] M. U. Arabul, M. Heres, M. C. Rutten, M. R. van Sambeek, F. N. van de Vosse, and R. G. Lopata, "Toward the detection of intraplaque hemorrhage in carotid artery lesions using photoacoustic imaging," *Journal of Biomedical Optics,* vol. 22, p. 041010, 2016.
[28] S. K. Kalva, P. K. Upputuri, and M. Pramanik, "High-speed, low-cost, pulsed-laser-diode-based second-generation desktop photoacoustic tomography system," *Optics Letters,* vol. 44, pp. 81-84, 2019.
[29] S. K. Kalva and M. Pramanik, "Use of acoustic reflector to make compact photoacoustic tomography system," *Journal of Biomedical Optics,* vol. 22, p. 026009, 2017.
[30] "American National Standard for Safe Use of Lasers ANSI Z136.1-2007 (American National Standards Institute, Inc., New York, NY, 2007)," ed.
[31] U. R. Chowdhury, B. H. Holman, and M. P. Fautsch, "A Novel Rat Model to Study the Role of Intracranial Pressure Modulation on Optic Neuropathies," *PLOS ONE,* vol. 8, p. e82151, 2013.
[32] S. Pomeranz, L. Beni, and M. N. Shalit, "The effect of intracranial hypotension on cerebral blood flow in a feline model," *Acta Neurochirurgica,* vol. 122, pp. 113-117, 1993.